Harmonic Suppression Induced by Three-Electron Dynamics of Li in Strong Laser Fields

Yu-Ning Yang,[1] Su-Qi Chen,[1] Zhao-Han Zhang◉,[1] Hui Jiang,[1] Min Chen,[1] Yang Li,[1,*] and Feng He[1,2,†]

[1]*Key Laboratory for Laser Plasmas (Ministry of Education) and School of Physics and Astronomy,*
Collaborative innovation center for IFSA (CICIFSA), Shanghai Jiao Tong University, Shanghai 200240, China
[2]*CAS Center for Excellence in Ultra-intense Laser Science, Shanghai 201800, China*

We build a model to elucidate the high harmonic generation in combined EUV and midinfrared laser fields by embodying the spin-resolved three-electron dynamics. The EUV pulse ionizes an inner-shell electron, and the midinfrared laser drives the photoelectron and steers the electron-ion rescattering. Depending on the spin of the photoelectron, the residual ion including two bound electrons can be either in a single spin configuration or in a coherent superposition of different spin configurations. In the latter case, the two electrons in the ion swap their orbits, leading to a deep valley in the harmonic spectrum. The model results agree with the time-dependent Schrödinger equation simulations including three active electrons. The intriguing picture explored in this work is fundamentally distinguished from all reported scenarios relied on spin-orbit coupling, but originates from the exchanges asymmetry of two-electron wave functions.

High harmonic generation (HHG) has attracted a lot of attention over the past few decades owing to its great potential for applications [1–4], for example, to synthesize attosecond pulses working as optical cameras to capture ultrafast chemical reactions with unprecedented time resolutions [5–7], to image electronic structures of atoms and molecules [8–14]. While HHG has been extensively studied in gases [15], very recently great efforts have also been paid for HHG in liquids [16,17] and solid materials [18–20]. In general, HHG in gases can be well explained by the well-established three-step model involving ionization, electron acceleration in the laser field, and recombination to the parent ion with the emission of a high-energy photon [21,22]. The three-step model has been extended to the four-step model in the HHG in solids [23,24].

One key assumption of the HHG process is the tunneling ionization of the outermost valence-shell electron in the first step. Considering the fact that tunneling ionization depends exponentially on the bound energy [25] and tightly bounded nature of the inner-shell electrons, usually, this assumption holds well and provides a clear picture of the measurable quantities. However, it may fail in two cases. First, when a few outer shells have very close ionization energies, an electron can tunnel out from multiple valence shells. For example, in molecules, depending on the molecular alignment with respect to the laser polarization direction, multiorbital contributions involving more than one electron have been experimentally demonstrated [26–29]. Second, the electron-electron correlation becomes dominant such that nonstationary hole transitions of the ionic states can not be neglected. For instance, using a time-dependent multiconfiguration self-consistent field method, Sato *et al.* [30] theoretically demonstrated that the electron correlation

effects must be properly taken into account in order to provide an accurate description of the atomic HHG process. Experimentally, for atoms, Shiner *et al.* [31] observed giant resonance in the HHG spectrum of Xe, revealing the importance of electron-electron interactions between the detached electron and deeply bound electrons. For molecules, Smirnova *et al.* [32] observed the attosecond hole transitions between the ionic states upon ionization of CO_2 and established high harmonic interferometry as an effective approach to resolving multielectron dynamics with sub-Ångström spatial resolution. The hole transition becomes very important especially when an EUV pulse participates in the ionization since the EUV pulse prefers knocking out an inner-shell electron and thus significantly increasing the number of possible channels in the HHG process [33,34].

For multielectron systems, the whole wave function including spin satisfies the exchange asymmetry. Different spin configurations associate with different spatial wave functions, which respond to external laser fields differently. An intuitive consequence one may expect is that the rescattering process and thus the harmonic generation depend on electron spin orientations. Very recently, Mayer *et al.* [35] reported time-resolved effects of spin-orbit coupling in HHG from argon by exciting dynamics of long-lived Rydberg trajectories. Their approach, where recombination occurs on the timescale of a few laser cycles, enabled them to explore spin-orbit coupling effects effectively [36].

In this Letter, taking Li in combined EUV and midinfrared (MIR) laser fields as an example, we develop a numerical model to calculate the HHG by including spin-resolved three-electron dynamics. We show, for the first time, how the spin dynamics of the ionic states affect HHG.
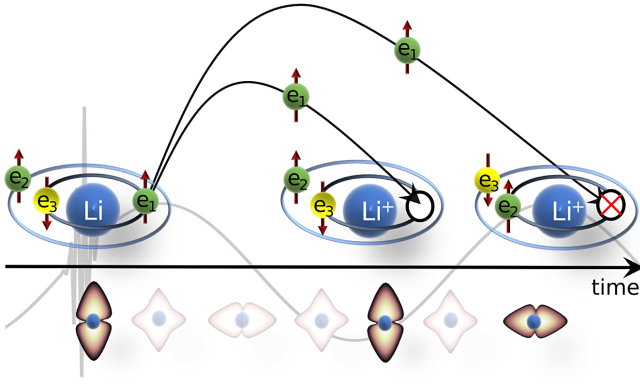
FIG. 1. Sketch of ionization and rescattering when the photoelectron is spin-up. The EUV MIR field is expressed by the gray curve. The Li and Li$^+$ are sketched by Bohr models. The time-evolved Li$^+$ wave functions are shown below the time axis. An inner-shell electron is freed by absorbing an EUV photon, and then is driven by the MIR field. Meanwhile, the wave functions below the time line show that the two electrons in two shells of Li$^+$ swap their orbits periodically. For different excursion times, the photoelectron may (the middle) or may not (the right, due to the Pauli principle) be recombined into the initial state.

For the convenience of discussion, we assume that two electrons are spin-up and one electron is spin-down. The target lithium is then labeled as Li($e_1^\uparrow, e_2^\uparrow, e_3^\downarrow$). As depicted in Fig. 1, upon the arrival of the EUV pulse, the inner-shell electron has a much larger cross section compared to the valence electron to absorb the EUV photon and gets freed [33,34,37]. Then the photoelectron is dragged back to the vicinity of the Li$^+$ by the MIR laser field. Depending on the spin of the photoelectron, the remaining two bound electrons located on different shells will have parallel or antiparallel spin orientations. In the latter case, the residual Li$^+$ is not in a single spin configuration, but a superposition of the singlet and triplet configurations. Such a superposition forms a quantum beat, leading to a periodic orbital swap of the two bound electrons in two shells. Depending on the excursion time of the photoelectron in the continuum, the initial inner-shell electron $e_3^\downarrow$, may hop to the shell $n = 2$ or return to the shell $n = 1$ at rescattering. If $e_3^\downarrow$ is in the shell $n = 2$ at the instant of rescattering, the state of Li$^+$ is orthogonal to the one just after the single ionization of Li, resulting in the annihilation of the dipole and the suppression of HHG emission. As a result, the local suppression in the HHG spectrum can be used to extract ultrafast spin-resolved multielectron dynamics. It is worthwhile to note here that in a pioneering work [38], Niikura *et al.* explored the HHG in a superposition of two electronic states using a single electron model. They found the attosecond bound-state wave packet dynamics are mapped onto the modulation of the HHG intensity. Here, we surpass this scope and study HHG from the many-electron atom Li. This involves a coherent superposition of spin singlet and

triplet states, driven by the multielectron spin symmetry, which is absent for a single-electron system.

Our model incorporates spin-resolved three-electron dynamics into the conventional Lewenstein model [39] based on strong field approximation. Several assumptions are made to simulate the process described in Fig. 1. First, the photoionization is only triggered by the EUV pulse. Second, the MIR pulse only drives the photoelectron in continuum states. Third, the Coulomb potential as well as the EUV field does not act on the photoelectron. Thus, the dipole moment induced by the laser fields is expressed as

$$\mathbf{d}(t) = -i \int^t dt' \langle g | \mathbf{r} e^{-i \int_{t'}^t [H_0 + H_{\mathrm{MIR}}(t'')] dt''}$$
$$\times H_{\mathrm{EUV}}(t') e^{iE_g(t-t')} | g \rangle + \mathrm{c.c.} \quad (1)$$

Here, $|g\rangle$ represents the ground state of Li, H_0 is the field-free atomic Hamiltonian, and $H_{\mathrm{MIR}} = \mathbf{r} \cdot \mathbf{E}_{\mathrm{MIR}}$ and $H_{\mathrm{EUV}} = \mathbf{r} \cdot \mathbf{E}_{\mathrm{EUV}}$ describe the MIR-Li and EUV-Li coupling, respectively, where $\mathbf{E}_{\mathrm{MIR}}$ and $\mathbf{E}_{\mathrm{EUV}}$ are the electric fields. $\mathbf{r}$ denotes the spatial coordinate of the photoelectron and E_g is the ground-state energy. In the derivation of Eq. (1), we have also neglected continuum-continuum transitions.

In the case that the photoelectron is spin-up, the remaining Li$^+$ is in a coherent superposition of the triplet state $|\eta\rangle = |1s2s^3S_{M_s=0}\rangle$ and singlet state $|\xi\rangle = |1s2s^1S\rangle$. For the ionization event at time t', the ionic wave function of Li$^+$ at a later time is expressed as

$$\psi_{\mathrm{Li}^+}(t, t') = \frac{1}{\sqrt{2}} e^{-iE_\eta(t-t')} |\eta\rangle - \frac{1}{\sqrt{2}} e^{-iE_\xi(t-t')} |\xi\rangle, \quad (2)$$

where E_η and E_ξ are the energies of triplet and singlet states, respectively. Together with the photoelectron, the produced wave function of the system (Li$^+$, $e_1^\uparrow$) can be written as

$$\Psi(t, t') = \frac{1}{\sqrt{2}} \int d\mathbf{p} |\mathbf{p} + \mathbf{A}_{\mathrm{MIR}}(t')\rangle \otimes |\eta\rangle e^{-i[S(t,t',\mathbf{p}) + E_\eta](t-t')}$$
$$- \frac{1}{\sqrt{2}} \int d\mathbf{p} |\mathbf{p} + \mathbf{A}_{\mathrm{MIR}}(t')\rangle \otimes |\xi\rangle e^{-i[S(t,t',\mathbf{p}) + E_\xi](t-t')},$$
$$(3)$$

where $S(t, t', \mathbf{p}) = \int_{t'}^t dt'' [\mathbf{p} + \mathbf{A}_{\mathrm{MIR}}(t'')]^2/2$, with $\mathbf{p}$ being the asymptotic drift momentum, is the classical action and $\mathbf{A}_{\mathrm{MIR}}(t) = -\int^t \mathbf{E}_{\mathrm{MIR}}(t') dt'$ is the vector potential of the MIR field. After lengthy but straightforward derivation from Eqs. (1) and (3), and using the saddle-point approximation to $\mathbf{p}$ yield (details can be found in Sec. 1 of Supplemental Material [40])

$$\mathbf{d}(t) = -i \sum_{j=\eta,\xi} \int^t dt' \left[\frac{\pi}{\epsilon + i(t-t')/2}\right]^{3/2} \mathbf{E}_{\text{EUV}}(t')$$
$$\times \mathbf{d}_j[\mathbf{p}_{st} + \mathbf{A}_{\text{MIR}}(t')]\mathbf{d}_j^*[\mathbf{p}_{st} + \mathbf{A}_{\text{MIR}}(t)]$$
$$\times e^{-i[S(t,t',\mathbf{p}_{st})+(E_j-E_g)(t-t')]} + \text{c.c.}, \quad (4)$$

where $\mathbf{d}_j(\mathbf{p})$ is the transition dipole associated with the ionic state $|j\rangle$ and $\mathbf{p}_{st} = -[1/(t-t')] \int_{t'}^t \mathbf{A}_{\text{MIR}}(t'')dt''$ is the saddle-point canonical momentum. Using a unitary transformation, we can rewrite Eq. (2) in a new basis set $|A\rangle = (1/\sqrt{2})(|\eta\rangle - |\xi\rangle)$ and $|B\rangle = (1/\sqrt{2})(|\eta\rangle + |\xi\rangle)$ as

$$\psi_{\text{Li}^+}(t,t') = \cos\left[\frac{\Delta E(t-t')}{2}\right]|A\rangle + i\sin\left[\frac{\Delta E(t-t')}{2}\right]|B\rangle, \quad (5)$$

where $\Delta E = E_\eta - E_\xi$. The coefficients $\cos[\Delta E(t-t')/2]$ and $\sin[\Delta E(t-t')/2]$ represent $e_2^\uparrow$ and $e_3^\downarrow$ hopping between the $n = 1$ and $n = 2$ shells periodically and ensure that at the ionization time t' the system is in the state $|A\rangle$. Using Eq. (5), we can change the summation index j in Eq. (4) to $j = A, B$. We arrive at our final expression of the dipole

$$\mathbf{d}(t) = -i \int^t dt' \cos\left[\frac{\Delta E(t-t')}{2}\right]\left[\frac{\pi}{\epsilon + i(t-t')/2}\right]^{3/2}$$
$$\times \mathbf{E}_{\text{EUV}}(t')\mathbf{d}_A[\mathbf{p}_{st} + \mathbf{A}_{\text{MIR}}(t')]\mathbf{d}_A^*[\mathbf{p}_{st} + \mathbf{A}_{\text{MIR}}(t)]$$
$$\times e^{-i[S(t,t',\mathbf{p}_{st})+I_p(t-t')]} + \text{c.c.}, \quad (6)$$

where $I_p = E_A - E_g$ is the ionization potential of state $|A\rangle$. Equation (6) is essentially identical to the Lewenstein model except for the additional factor $\cos[\Delta E(t-t')/2]$ which represents the orbital swap process. The HHG spectra are computed as the squared modulus of the Fourier-transformed electric dipole acceleration. The dipole acceleration $a_1(t)$ of photoelectron $e_1^\uparrow$ is obtained as the second derivative of the dipole moment in Eq. (6). As a comparison, when the photoelectron is spin-down, marked as $e_3^\downarrow$, the remaining two electrons $(e_1^\uparrow, e_2^\uparrow)$ in Li$^+$ have parallel spin orientations. Li$^+$ is in a triplet state and no orbital swap occurs. The dipole acceleration $a_3(t)$ of $e_3^\downarrow$ is thus obtained by the conventional Lewenstein model, which works as a reference.

To demonstrate the availability of our model, we also simulate the time-dependent Schrödinger equation (TDSE) including three active electrons of Li. The three-electron wave function is written as

$$\Psi(q_1, q_2, q_3) = \Theta[\alpha(1)\alpha(2)\beta(3)\Phi_{\alpha\alpha\beta}(\mathbf{r}_1, \mathbf{r}_2, \mathbf{r}_3)]. \quad (7)$$

Here, q_i is the spin-spatial coordinate, $\mathbf{r}_i$ is the spatial coordinate, $\alpha(i)$ and $\beta(i)$ represent spin-up and spin-down states, and Φ is the spatial wave function. Θ performs the cyclic sum $\Theta[f(1,2,3)] = [f(1,2,3) + f(2,3,1) + f(3,1,2)]/\sqrt{3}$ for arbitrary f. $\Phi_{\alpha\alpha\beta}(\mathbf{r}_1, \mathbf{r}_2, \mathbf{r}_3)$ is the spatial

wave function associated with the spin $\alpha(1)\alpha(2)\beta(3)$, i.e., $(e_1^\uparrow, e_2^\uparrow, e_3^\downarrow)$, and it is antisymmetric under the exchange of $\mathbf{r}_1$ and $\mathbf{r}_2$. Fully describing each electron in three dimensions is out of the capability of most advanced computers, and a plausible way is to confine the movement of each electron in one dimension, although such a treatment still brings heavy calculations. In the reduced-dimensionality model, the exchange asymmetry is perfectly preserved, and thus this model can be used to qualitatively describe the main dynamics discussed in this topic. The governed TDSE in the velocity gauge is (atomic states are used throughout unless stated otherwise)

$$i\frac{\partial}{\partial t}\Phi_{\alpha\alpha\beta}(x_1, x_2, x_3; t) = [H_0 + W(t)]\Phi_{\alpha\alpha\beta}(x_1, x_2, x_3; t), \quad (8)$$

where H_0 is the field-free Hamiltonian

$$H_0 = -\sum_{i=1}^3 \frac{\partial^2}{2\partial x_i^2} - \sum_{i=1}^3 \frac{3}{\sqrt{x_i^2 + s_1}}$$
$$+ \sum_{i=1}^3 \sum_{j=1}^{i-1} \frac{1}{\sqrt{(x_i - x_j)^2 + s_2}}, \quad (9)$$

and $W(t) = \Sigma_{i=1}^3[-iA(t)(\partial/\partial x_i)]$ is the laser interaction term. The soft-core parameters are set as $s_1 = 0.5$ and $s_2 = 2.0$ and closely give the ionization potential of these two states of $|\eta\rangle$ and $|\xi\rangle$ in real Li$^+$, which play the key role in the underlying physical process considered in the present study. The energy levels of our model are provided in Supplemental Material [40]. According to Ehrenfest theorem [41], the dipole acceleration is

$$a_i(t) = \langle\Phi_{\alpha\alpha\beta}(t)| - \frac{\partial V_0}{\partial x_i} - E(t)|\Phi_{\alpha\alpha\beta}(t)\rangle, \quad (10)$$

where V_0 represents the Coulomb interaction in Eq. (9) and $E(t)$ is the electric field. In the TDSE simulations, the spatial steps are $\delta x_1 = \delta x_2 = \delta x_3 = 0.4$ a.u., and the time step is $\delta t = 0.05$ a.u. Each dimension covers the space $[-320 \text{ a.u.}, 320 \text{ a.u.}]$. A mask function $\cos^{1/6}$ is used in borders to suppress the unphysical reflections from boundaries [42]. The initial state is numerically obtained via the imaginary time propagation, and the wave function propagation in real time is calculated using Crank-Nicholson method. The spin-resolved HHG spectrum is obtained via $\tilde{a}_i(\omega) = (1/\sqrt{2\pi}) \int a_i(t)e^{-i\omega t}dt$.

To elucidate the orbital swap process in TDSE simulation, we first record the time evolution of Li$^+$ after $e_1^\uparrow$ is ionized at a series of instants by TDSE simulation, as shown in Fig. 2. These snapshots explicitly show the two bound electrons periodically swap their positions with the period of about $T_p = 78$ a.u.
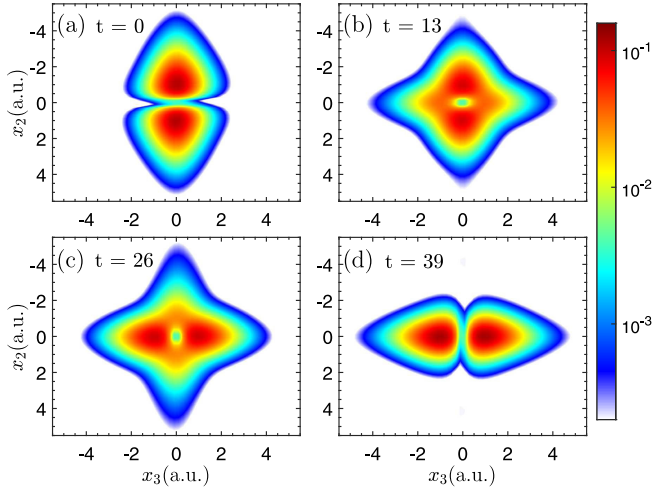
FIG. 2. Snapshots of electron density distributions of the Li$^+$ in the x_2-x_3 plane at different instants.
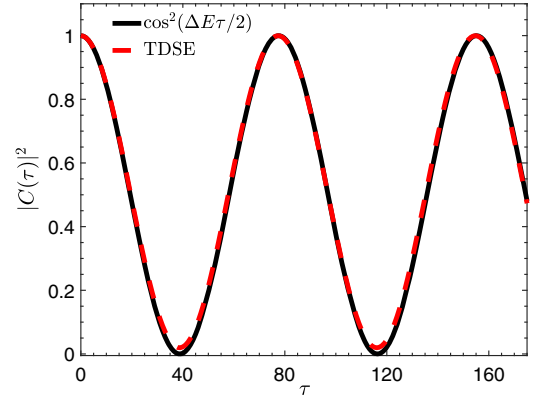

FIG. 3. The modulus square of autocorrelation function $|C(\tau)|^2$ (red dashed curve) extracted from TDSE simulation. The factor $\cos^2(\Delta E\tau/2)$ (black solid curve) incorporated in our Lewenstein model is also shown for comparison.

The coefficient which represents the orbital swap in Eq. (6) can also be extracted from TDSE simulation. We can define the autocorrelation function

$$C(\tau) = \langle \psi_{\mathrm{Li}^+}(t') | \psi_{\mathrm{Li}^+}(t) \rangle, \qquad (11)$$

where $\psi_{\mathrm{Li}^+}(t')$ is the wave function of Li$^+$ after the sudden removal of an inner-shell up-spin electron and $\tau = t - t'$ is the excursion time. Figure 3 compares the consistency of the autocorrelation function and the coefficient from our incorporated Lewenstein model. As the orbital swap picture is naturally described in TDSE simulation, the agreement between $|C(\tau)|^2$ and $|\cos(\Delta E\tau/2)|^2$ indicates that it is feasible to describe the orbital swap process with Eq. (6). At this stage, we would like to emphasize again here that if the photoelectron is spin-down ($e_3^\downarrow$), the remaining two bound electrons in Li$^+$ are both spin-up. Such a spin triplet state does not lead to orbital swap in Li$^+$.

We now show how the orbital swap process manifest itself in the HHG. The vector potential of the combined EUV and MIR laser fields is written as

$$A(t) = A_{\mathrm{MIR}} \cos(\omega_{\mathrm{MIR}} t) \cos^2\left(\frac{t}{\tau_{\mathrm{MIR}}}\right)$$
$$+ A_{\mathrm{EUV}} \cos\left[\omega_{\mathrm{EUV}}(t - \Delta t)\right] \exp\left[-4\ln 2 \left(\frac{t - \Delta t}{\tau_{\mathrm{EUV}}}\right)^2\right], \qquad (12)$$

where ω_{MIR} and ω_{EUV} are the angular frequencies of the MIR and EUV pulses, respectively, and Δt denotes the time delay. In our calculations, the MIR field has a wavelength of 3000 nm, the intensity of 2×10^{13} W/cm^2, and the pulse lasts for two optical cycles, i.e., $\tau_{\mathrm{MIR}} = 4\pi/\omega_{\mathrm{MIR}}$. The EUV pulse has the central frequency of 3.2 a.u., the pulse duration $\tau_{\mathrm{EUV}} = 15.7$ a.u. (380 attoseconds) and the

intensity of 10^{16} W/cm^2. We note that using such a high intensity is only for increasing the signal-to-noise ratio, a much weaker EUV intensity will bring similar physical results. We also confirm that this EUV pulse mainly ionizes the inner-shell electron and makes the ionization path leaving the Li$^+$ cation in the configuration of $1s2s$ the dominant one (see Secs. 2 and 3 of Supplemental Material [40]). Moreover, by choosing a proper time delay between the EUV and MIR pulses, we can conclude that only in this path, the photoelectron can be driven back by the MIR pulse and thereby has contributions to HHG. Other channels, for instance, the electron ionized from $n = 2$ orbital, is too energetic to recombine, and no high harmonics are emitted. In the following calculations, we set $\Delta t = 20$ a.u.

The calculated HHG spectra in the combined EUV and MIR laser fields are shown in Fig. 4(a). The red solid curve is for the spin-up photoelectron obtained by our incorporated Lewenstein model. The big hump around 80–100 eV is contributed by the EUV pulse itself, and the part with an energy lower than 70 eV is contributed by rescattering steered by the MIR pulse. A distinct valley at around 62 eV in the spectrum is observed. In contrast, the HHG spectrum for down-spin photoelectron (light red strip) is continuous over this region due to the absence of orbital swap. Figure 4(a) also shows the HHG obtained from the TDSE simulation for the case that the photoelectron is spin-up (black solid) or spin-down (light black strip). The TDSE simulation results have been shifted vertically to separate from the incorporated Lewenstein model results for clear visualization. The model results and the TDSE simulation results show almost the same structures.

The valley at around 62 eV in the HHG spectrum is indeed contributed by the term $\cos[\Delta E(t - t')/2]$ in Eq. (6), which can be confirmed by diagnosing the time-frequency analysis of the dipole acceleration by Gabor transformation. Figures 4(b) and 4(c) show the time-frequency spectrograms simulated by our incorporated Lewenstein
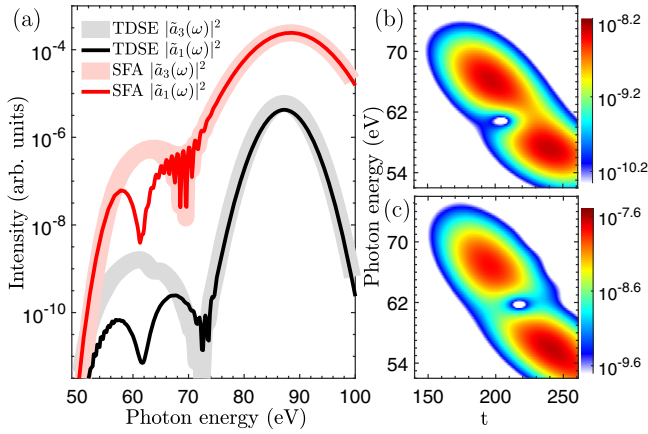
FIG. 4. (a) High harmonic spectra of Li in a combined EUV and MIR laser field. (b) and (c) Time-frequency maps of HHG, calculated by the incorporated Lewenstein model and TDSE, respectively.

model and TDSE, respectively. As one can see, the time delay is properly adjusted such that only one trajectory is responsible for HHG in the region of 50–80 eV. This allows us to define a single time-energy mapping to relate the minimum to the HHG emission time. In our calculations, the attosecond EUV pulse appears at $t' = 20$ a.u., which can be regarded as the single ionization instant since the EUV pulse is very short. Figures 4(b) and 4(c) show distinct minimum at around $t = 215$ a.u., which indicates the corresponding photoelectron excursion time of 195 a.u. According to the autocorrelation function, if the excursion time $t - t'$ is $(N + 1/2)T_p$ (N is an integer), the harmonic is significantly suppressed. By setting $N = 2$, such analysis indeed suggests the harmonic suppression at $t = 215$ a.u.

The experimental realization of the present scenario may need the spin of the ionized electron to be determined in advance. This can be achieved, for example, by Mott detectors [43], although now it still suffers from low detection efficiencies. However, we would like to note that such a valley can also be observed in experiments without measuring the spin of the ionized electron. Exposing Li atoms in the EUV MIR fields, the spin-up and spin-down electrons in the shell $n = 1$ almost have the same ionization cross section, and the observed HHG should be $S(\omega) = |\sum_{i=1}^{3} \tilde{a}_i(\omega)|^2$. Whatever the spin of Li atoms, the single-ionization pathway induced orbital swap in Li$^+$ always exists, thus for trajectories having the excursion time $(N + 1/2)T_p$ can always lead to local harmonic suppression. By changing the time delay between EUV and MIR pulses, the local valley can be controlled.

To summarize, we develop an incorporated Lewenstein model to study the HHG of Li, which is comparable with the TDSE simulation results. The multielectron dynamics can be included by adding the $\cos[\Delta E(t - t')/2]$ function, which neatly describes the orbital swap of the electron in Li$^+$. We would like to put the emphasis on the orbital swap

of two electrons, clarifying that it is distinct from the spin-orbit coupling mentioned in previous studies [35,36]. Instead, this phenomenon solely depends on the exchange asymmetry between the two electrons. The orbital swap leads to a local valley in HHG, which can be inversely used to retrieve ultrafast electron dynamics in atoms. We expect such scenarios to occur not only in Li, but also in many atoms or molecules with open-shell structures.

*liyang22@sjtu.edu.cn
†fhe@sjtu.edu.cn

[1] P. B. Corkum and F. Krausz, Nat. Phys. **3**, 381 (2007).
[2] F. Krausz and M. Ivanov, Rev. Mod. Phys. **81**, 163 (2009).
[3] L. Gallmann, C. Cirelli, and U. Keller, Annu. Rev. Phys. Chem. **63**, 447 (2012).
[4] F. Calegari, G. Sansone, S. Stagira, C. Vozzi, and M. Nisoli, J. Phys. B **49**, 062001 (2016).
[5] M. Chini, K. Zhao, and Z. Chang, Nat. Photonics **8**, 178 (2014).
[6] T. Gaumnitz, A. Jain, Y. Pertot, M. Huppert, I. Jordan, F. Ardana-Lamas, and H. J. Wörner, Opt. Express **25**, 27506 (2017).
[7] P. Tzallas, E. Skantzakis, L. Nikolopoulos, G. D. Tsakiris, and D. Charalambidis, Nat. Phys. **7**, 781 (2011).
[8] F. Lépine, M. Y. Ivanov, and M. J. Vrakking, Nat. Photonics **8**, 195 (2014).
[9] M. Nisoli, P. Decleva, F. Calegari, A. Palacios, and F. Martín, Chem. Rev. **117**, 10760 (2017).
[10] A. Palacios and F. Martín, Comput. Mol. Sci. **10**, e1430 (2020).
[11] J. Itatani, J. Levesque, D. Zeidler, H. Niikura, H. Pépin, J.-C. Kieffer, P. B. Corkum, and D. M. Villeneuve, Nature (London) **432**, 867 (2004).
[12] C. Vozzi, M. Negro, F. Calegari, G. Sansone, M. Nisoli, S. De Silvestri, and S. Stagira, Nat. Phys. **7**, 822 (2011).
[13] S. Haessler, J. Caillat, W. Boutu, C. Giovanetti-Teixeira, T. Ruchon, T. Auguste, Z. Diveki, P. Breger, A. Maquet, B. Carré, R. Taïeb, and P. Salières, Nat. Phys. **6**, 200 (2010).
[14] H. J. Wörner, J. B. Bertrand, P. Hockett, P. B. Corkum, and D. M. Villeneuve, Phys. Rev. Lett. **104**, 233904 (2010).
[15] R. Weissenbilder, S. Carlström, L. Rego, C. Guo, C. M. Heyl, P. Smorenburg, E. Constant, C. L. Arnold, and A. L'Huillier, Nat. Rev. Phys. **4**, 713 (2022).
[16] T. T. Luu, Z. Yin, A. Jain, T. Gaumnitz, Y. Pertot, J. Ma, and H. J. Wörner, Nat. Commun. **9**, 1 (2018).
[17] A.-W. Zeng and X.-B. Bian, Phys. Rev. Lett. **124**, 203901 (2020).
[18] S. Ghimire and D. A. Reis, Nat. Phys. **15**, 10 (2019).
[19] T. Heinrich, M. Taucer, O. Kfir, P. Corkum, A. Staudte, C. Ropers, and M. Sivis, Nat. Commun. **12**, 1 (2021).

[20] E. Goulielmakis and T. Brabec, Nat. Photonics **16**, 411 (2022).

[21] J. L. Krause, K. J. Schafer, and K. C. Kulander, Phys. Rev. Lett. **68**, 3535 (1992).

[22] P. B. Corkum, Phys. Rev. Lett. **71**, 1994 (1993).

[23] L. Li, P. Lan, X. Zhu, T. Huang, Q. Zhang, M. Lein, and P. Lu, Phys. Rev. Lett. **122**, 193901 (2019).

[24] T. Ikemachi, Y. Shinohara, T. Sato, J. Yumoto, M. Kuwata-Gonokami, and K. L. Ishikawa, Phys. Rev. A **95**, 043416 (2017).

[25] M. V. Ammosov, N. B. Delone, and V. P. Krainov, High Intensity Laser Process. **664**, 138 (1986).

[26] B. K. McFarland, J. P. Farrell, P. H. Bucksbaum, and M. Guhr, Science **322**, 1232 (2008).

[27] A.-T. Le, R. Lucchese, and C. Lin, J. Phys. B **42**, 211001 (2009).

[28] G. H. Lee, I. J. Kim, S. B. Park, T. K. Kim, Y. S. Lee, and C. H. Nam, J. Phys. B **43**, 205602 (2010).

[29] Z. Shu, H. Liang, Y. Wang, S. Hu, S. Chen, H. Xu, R. Ma, D. Ding, and J. Chen, Phys. Rev. Lett. **128**, 183202 (2022).

[30] T. Sato, K. L. Ishikawa, I. Březinová, F. Lackner, S. Nagele, and J. Burgdörfer, Phys. Rev. A **94**, 023405 (2016).

[31] A. Shiner, B. Schmidt, C. Trallero-Herrero, H. J. Wörner, S. Patchkovskii, P. B. Corkum, J. Kieffer, F. Légaré, and D. Villeneuve, Nat. Phys. **7**, 464 (2011).

[32] O. Smirnova, Y. Mairesse, S. Patchkovskii, N. Dudovich, D. Villeneuve, P. Corkum, and M. Y. Ivanov, Nature (London) **460**, 972 (2009).

[33] C. Buth, F. He, J. Ullrich, C. H. Keitel, and K. Z. Hatsagortsyan, Phys. Rev. A **88**, 033848 (2013).

[34] A. C. Brown and H. W. van der Hart, Phys. Rev. Lett. **117**, 093201 (2016).

[35] N. Mayer, S. Beaulieu, A. Jiménez-Galán, S. Patchkovskii, O. Kornilov, D. Descamps, S. Petit, O. Smirnova, Y. Mairesse, and M. Y. Ivanov, Phys. Rev. Lett. **129**, 173202 (2022).

[36] S. Pabst and R. Santra, J. Phys. B **47**, 124026 (2014).

[37] A. S. Kheifets, D. V. Fursa, and I. Bray, Phys. Rev. A **80**, 063413 (2009).

[38] H. Niikura, D. M. Villeneuve, and P. B. Corkum, Phys. Rev. Lett. **94**, 083003 (2005).

[39] M. Lewenstein, P. Balcou, M. Y. Ivanov, A. L'Huillier, and P. B. Corkum, Phys. Rev. A **49**, 2117 (1994).

[40] See Supplemental Material at http://link.aps.org/supplemental/10.1103/PhysRevLett.131.183201 for (1) derivation of the incorporated strong-field approximation model, (2) comparison of single and double ionization probabilities, (3) investigation of high harmonic generation with a weaker assisted EUV pulse, (4) analysis of energy levels and cation populations of the one-dimensional model, and (5) exploration of the potential for experimental realization.

[41] K. Burnett, V. C. Reed, J. Cooper, and P. L. Knight, Phys. Rev. A **45**, 3347 (1992).

[42] F. He, C. Ruiz, and A. Becker, Phys. Rev. A **75**, 053407 (2007).

[43] S. Souma, A. Takayama, K. Sugawara, T. Sato, and T. Takahashi, Rev. Sci. Instrum. **81**, 095101 (2010).